Available online at www.sciencedirect.com

ScienceDirect

Procedia Engineering 10 (2011) 1170–1175

Engineering Procedia

ICM11

Corrosion Fatigue Crack Propagation of High-strength Steel HSB800 in a seawater environment

Dong-Hwan Kang[a], Jong-Kwan Lee[b], Tae-Won Kim[a,*]

[a]School of Mechanical Engineering, Hanyang University, 17 Haengdang-dong, Seongdong-gu, Seoul 133-791, Republic of Korea
[b]Steel structure Research Institute of Industrial Science & Technology, Hwaseong 445-813, Republic of Korea

Abstract

Fatigue and corrosion fatigue crack propagation behaviors of high-strength steel, HSB800, were investigated in air and seawater environments. Three-point bending fatigue tests were conducted under various loading conditions at different levels of load frequency and ratio. A fracture model enabling mechanisms-based prediction of corrosion fatigue crack propagation is presented. The results obtained from the model follow the experimental data very well. Validation of the model was also conducted by comparison with other models that used in the analyses of corrosion fatigue crack propagation rates. As shown in results, the corrosion fatigue crack propagation rates in a seawater environment were higher than those in air condition under every loading conditions. These higher corrosion fatigue crack propagation rates were made possibly by the mechanisms of hydrogen embrittlement together with anodic dissolution.

Keywords: Corrosion fatigue; Crack propagation; Fracture mechanics; Seawater; High strength steel

1. Introduction

Currently, high performance steel, HSB800 for long-span bridges has been developed by means of a thermo-mechanically controlled process (TMCP). This manufactured steel showed a remarkably improved mechanical strength, good weldability and good weather resistance as well [1]. Due to the increasing usage and severe in service conditions such as cyclic loading under extreme weather, external massive loads, and corrosive marine environment, much more accurate analysis of the material-mechanics characteristics, particularly the corrosion fatigue behavior is required.

In open, corrosion fatigue life of structural members can be classified into two steps: the corrosion fatigue crack initiation (CFCI) life and the corrosion fatigue crack propagation (CFCP) life. Usually, the longer part of life time for the structures is covered by CFCP instead of CFCI [2,3]. The CFCP mechanism is similar to the stress corrosion cracking (SCC). Even though the mechanism of SCC is not clear, it is usually explained by hydrogen embrittlement. Here, the CFCP rate is considered to be an accelerated crack propagation rate of SCC promoted in a certain corrosive environment by cyclic loading. Two possible mechanisms such as anodic dissolution and hydrogen embrittlement are adopted to describe the acceleration of crack propagation rate at corrosive environment.

Determination of the effects of corrosion environment on the behavior had been done by the measuring of the CFCP rate against the fatigue crack propagation (FCP) rate. The empirical Paris equation is still employed for the analysis of FCP rate [3-5]. It is recognized that the parameters in Paris equation are fitting coefficients obtained by experimental data, and thus it is not easy to define the mechanism based influence such as grain bridging, oxide wedging, micro void coalescence, cleavage fracture, hydrogen embrittlement and etc. [6]. In connection with Paris model, the NASGRO equation representing the three general FCP behaviors such as region I, II and III has widely been applied in the prediction of crack propagation life [7]. Only a few number of mathematical expressions for the CFCP rate, however have been suggested in the CFCP life estimation pending on empirical expressions [3,8] since the mechanism of the CFCP also has not been clearly identified.

* Corresponding author. Tel.: +82-2-2220-0421; fax: +82-2-2292-0401.
E-mail address: twkim@hanyang.ac.kr.

1877-7058
Selection and peer-review under responsibility of ICM11 doi:10.1016/j.proeng.2011.04.195

Table 1. Chemical composition and mechanical properties of HSB800

Chemical composition	C	Si	Mn	P	S	Cu	Cr	Ni
	≤ 0.10	≤ 0.65	≤ 2.20	≤ 0.015	≤ 0.006	0.10-0.50	0.45-0.75	0.05-0.80
Mechanical properties	YS		UTS		E		elongation	
	≥ 690 MPa		≥ 800 MPa		205 GPa		≥ 16%	

The major thrust of this paper is, therefore, modeling the CFCP behavior of high strength steels, particularly in a seawater environment comparing with an air condition. In order to develop the mechanism-based life prediction model, and also to characterize the FCP together with the CFCP behaviors, fatigue tests were conducted with a three-point, single-edge notched bending (SENB-3) fixture. To this fixture, three types of load conditions, such as load frequency and minimum/maximum load ratio were applied. A mathematical expression of the CFCP rate of HSB800 in seawater modified using the Forman equation was then presented. This newly developed model demonstrates the effect of a corrosive environment on the CFCP behavior and also the effect of a load frequency on the FCP and the CFCP behaviors. In addition, the new model was validated by comparing its results through the work with the fitting curves obtained from other common equations.

2. Experiments

High strength steel, HSB800, produced by TMCP for long-span bridges was used as the base metal. The chemical composition and mechanical properties are summarized in Table 1. Single-edge notched bending (SENB) specimens of 10 mm x 20 mm cross-section were extracted from the rolled-plates with the notch in L-T orientation.

FCP tests in which the ΔK envelope increased were conducted in air and 3.5% sodium chloride (NaCl) solution The test was conducted by using an universal 50 kN mechanical testing machine at room temperature. The machine was equipped with a digital controller interfaced to a personal computer. A pre-cracking after wire cutting technique was used with every specimen. In order to prevent an undesirable chemical reaction between NaCl solution and the testing stuffs, an acryl container with inverted three point bend fixture was used. Loading jigs and three rollers contacting to specimen were made up with stainless steel and Teflon, respectively. A schematic diagram for this test fixture is shown in Figure 1a.

The evolution of crack length was directly measured using a KV-5C (KYOWA ELECTRONIC INSTRUMENTS CO., LTD) crack gauge. This gauge, attached to the surface of the specimen, measures the crack length by the existing number of copper wires. The three types of loading condition are summarized in Figure 1b. As can be seen, the load frequency, f, and load ratio, R were varied from 0.1 to 0.5 by employing the triangular waveforms.

3. Corrosion fatigue crack propagation models

3.1. Relevant models for fatigue crack propagation process

As it is known, the Paris model, $da/dN = C_P(\Delta K)^{m_P}$, identified the FCP behavior by using the relationship between crack propagation rate, da/dN and the range of the stress intensity factor (SIF), ΔK with the coefficient, C_P and the exponent, m_P. This equation covers only the stable FCP in region II. The overall FCP behaviors under cyclic loading thus cannot be adequately characterized by the Paris model alone. As an extension to the Paris equation, Forman [9] proposed a FCP model covering the region II and the instable FCP region III as well by taking the critical SIF, K_{crit} as follows:

$$\frac{da}{dN} = \frac{C_F(\Delta K)^{m_F}}{(1-R)K_{crit} - \Delta K} \tag{1}$$

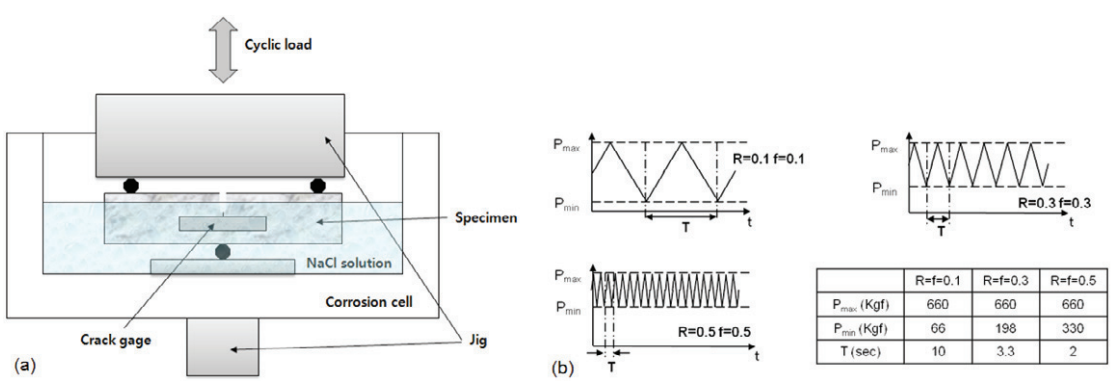

Fig. 1. Schematic diagrams showing the (a) experimental apparatus for the CFCP test and (b) summary of loading conditions.

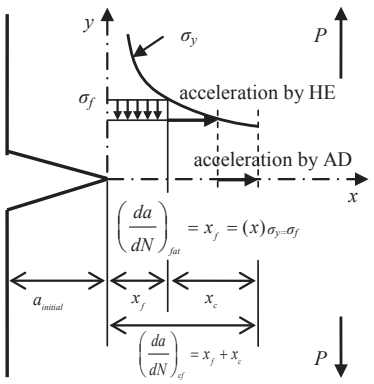

Fig. 2. Schematic diagram showing the corrosion fatigue crack propagation process [8].

where R is the ratio of minimum and maximum applied loads, C_F and m_F are the material constants. However, the Forman equation is still not sufficient to represent the overall FCP behavior. Thus, after many attempts, NASA, namely NASGRO equation, proposed a good fitting method for the FCP behavior. It covers all the regions, I, II and III, and also the effect of load ratio [7].

$$\frac{da}{dN} = C_N \left(\frac{1-Q}{1-R} \Delta K \right)^{m_N} \left(1 - \frac{\Delta K_{th}}{\Delta K} \right)^{p} \Bigg/ \left(1 - \frac{K_{\max}}{K_{crit}} \right)^{q} \tag{2}$$

where C_N, m_N, p, q are the fitting constants, Q is the ratio of the crack opening SIF, K_{op}, and maximum SIF in each loading cycle, K_{max} as to be $Q=K_{op}/K_{max}$, and ΔK_{th} is threshold value of SIF range. The NASGRO equation, however, has too much fitting parameters so that, it is hard to clearly identify the significance of each fitting constants to the mechanical/environmental effect on the FCP curve. Also the above equations do not include any factor that related to loading frequency. Therefore, the fitting constants should be defined for every different mechanical load and environmental conditions.

By the comparison with those models, relatively simple and effective Forman equation due to less number of fitting constants which enabling the identification of the relationship between environmental effects and fitting constants, has been considered. A modified model based on Forman equation including the loading frequency and environmental factors thus has been developed as below.

3.2. Modeling the fatigue crack propagation

Forman's equation could not describe the FCP region I by the relatively low ΔK. Thus Hartman and Schijve [10] proposed a modified equation by the consideration of ΔK_{th} effect. Furthermore, Elber [11] assumed that the amount of contact crack surface (i.e., crack closure) during a loading cycle decreases the effective SIF range resulting in the decrease of FCP rate, simultaneously. When a specimen applied to cyclic load through the maximum and minimum SIF, FCP occurs only if the current SIF level is larger than the crack opening SIF. Thus the effective SIF range can be expressed as $\Delta K_{eff} = K_{\max} - K_{op} = U\Delta K$ where U is the ratio of effective SIF range.

In this work, the ratio of effective SIF range was contemplated in Eqn. (1) to increase the accuracy as follow:

$$\frac{da}{dN} = \frac{C(f)\left[U\left(\Delta K - \Delta K_{th}\right)\right]^{m(f)}}{U\left[(1-R)K_{crit} - \Delta K\right]} \tag{3}$$

where $C(f)$ and $m(f)$ are material parameters and U is to be $U=a+bR$., and where a, b are empirically determined material constants. The effect of loading frequency, f, was implemented into the equation by the parameters C and m as

Table 2. Summary of material constants.

Model	Constants	*R=f=0.1* (Air/NaCl)	*R=f=0.3* (Air/NaCl)	*R=f=0.5* (Air/NaCl)
NASGRO	m_N	0.7/1.0	0.3/1.22	0.22/1.41
	C_N	2.3E-9/8.1E-8	2.1E-8/1.4E-9	1.6E-8/4.4E-10
	p	0.14/1.42	0.04/1.01	0.01/0.95
	q	0.40/0.03	0.90/0.31	0.91/0.41
WANG	B_{cf}	/1.1E-7	/4.2E-8	/4.5E-8
Eqn. (3)	m	0.32/1.1	0.17/0.94	0.03/0.93
	C	8.9E-6/5.1E-5	7.9E-6/9.1E-6	3.8E-6/6.2E-6

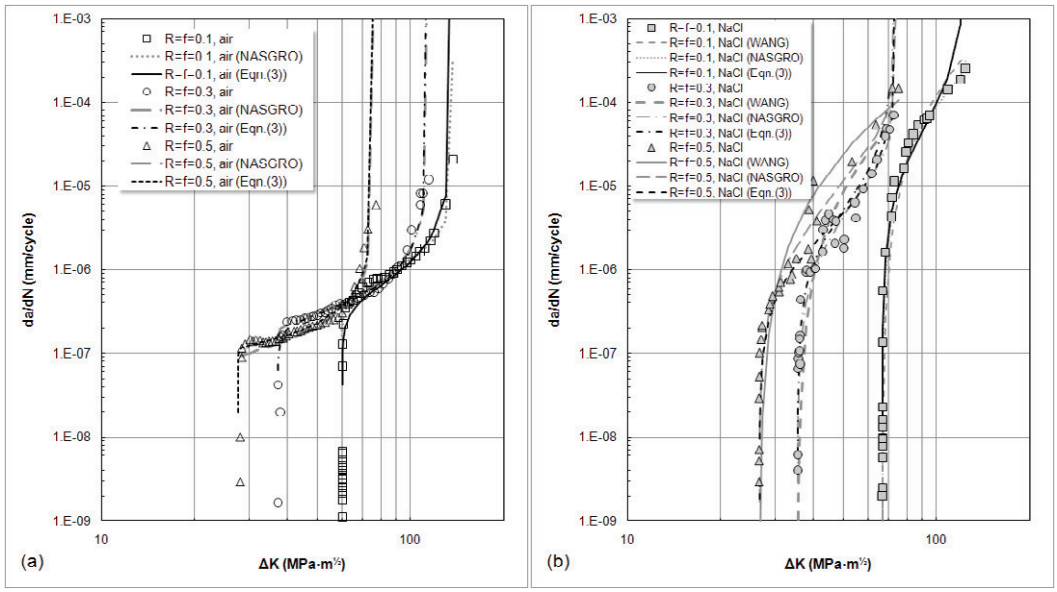

Fig. 3. Experimentally measued FCP and CFCP behaviors of HSB800 and fitting curves by using the equations for the (a) air and (b) NaCl solution conditions.

$C(f) = \alpha \exp(\beta f)$; $m(f) = \gamma \ln f + \delta$, where α, β, γ and δ are material constants. The relationships between *f* and parameters had been found by using the experimental data and least square curve fitting method. Materials constants used in this work are summarized in Table 2.

3.3. Modeling the corrosion fatigue crack propagation

It is believed that the CFCP is caused by the combination of corrosion damage and relative slip of the metal at the crack tip under cyclic loading. This process is controlled by the three major mechanisms: relative slip of the metal at the crack tip, the bare surface corrosion of the fractured material elements and the crack closure. The corrosion in the CFCP process occurs mainly on the bare surface after the material elements are fractured [8].

In aqueous environment, two possible mechanisms are associated with the corrosion damage on the CFCP process: anodic dissolution (AD) at the crack tip, and hydrogen penetration by AD into the material elements resulting in hydrogen embrittlement (HE). In consequence, both AD and HE lead out the acceleration of crack propagation where is not the case of air environment [12,13].

As shown in Figure 2, a material element exposing crack tip can be fractured by applied load, *P* when the level of stress at the crack tip reaches failure strength of the material. Only considering the stress effect without any corrosion such as FCP in a cyclic loading hysteresis, following processes occur: crack opening by increasing load - crack propagation due to fracture of the material element at crack tip - crack closing by decreasing load - crack opening [6]. However, in a corrosive environment, CFCP may occur by the processes: crack opening by increasing load - longer crack propagation due to decrease of failure strength by HE - additional crack propagation with blunting at the crack tip by AD - crack closing by decreasing load - crack opening [8].

Also, the FCP length in a cyclic load can be expressed as $\left(da/dN\right)_{fat} = x_f = (x)_{\sigma_y = \sigma_f}$, where σ_y and σ_f are the yield (flow) stress and failure strength of the material element, respectively. Meanwhile, the CFCP will be accelerated by two different mechanisms, HE and AD in the corrosive environment as mentioned above. Total amount of the CFCP length in a cyclic load therefore gives the CFCP rate as the equation, $\left(da/dN\right)_{cf} = x_f + x_c$, shown in Figure 2. $\left(da/dN\right)_{cf}$ is the CFCP rate, x_f is the length of crack propagation in a loading cycle and x_c is the length of additional crack propagation in a cycle due to the corrosive environment. Wang [8] proposed a CFCP rate model for aluminum alloys at 3.5% NaCl as $\left(da/dN\right)_{cf} = B_{cf}\left(\Delta K - \Delta K_{thcf}\right)^2$, where B_{cf} is the coefficient of the CFCP and ΔK_{thcf} is the CFCP threshold of SIF range. This Wang equation is one of the very few CFCP models, but the equation still has limitation on fitting the region III and the changing slope according to varying load conditions due to the fixed exponent constant at two. Also, the effect of load frequency was not considered in the equation properly. Therefore, a new fracture model which can describe both the FCP and the CFCP behaviors was required to establish the signification of the parameters related to environmental effects.

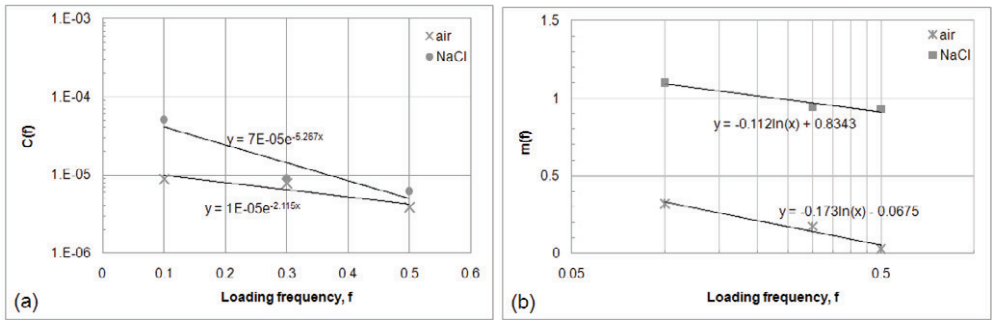

Fig. 4. Relationships between loading frequency and material parameters; (a) *C(f)* and (b) *m(f)*.

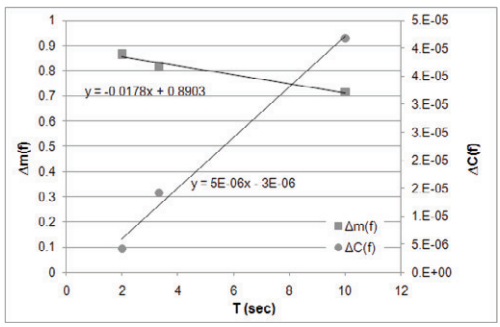

Fig. 5. Relationships between time period and both *ΔC(f)* and *Δm(f)*.

In this work, a degradation of the CFCP resistance due to the corrosive environment was considered by means of the possible corrosion mechanisms such as HE and AD corresponding to the parameters *m(f)* and *C(f)* in Eqn. (3). The degradation of material strength may be limited to a certain level of failure strength according to the saturation of hydrogen concentration level at the specimen's surface. Thus, the degradation effect by HE to the failure strength mostly depends on the initial exposure time. On the other hand, the effect of AD on the CFCP can be steadily increased or held during the exposure time in the corrosive solution. Nevertheless, if the quantitative relationship between the parameters and the exposure time can be identified by the experimental data, it is possible to give the qualitative relations between the corrosion mechanisms and the parameters.

4. Results and discussions

4.1. Experimental results

Figure 3a and 3b show the experimentally measured the FCP and CFCP behaviors of HSB800 under various loading conditions in air and NaCl solution, respectively. As can be seen, the FCP rates are dramatically increased in NaCl solution than in air for every mechanical loading condition. Also the behaviors show that the region I and II could be clearly indentified in both air and NaCl environment. The region III however was hard to identify at NaCl condition. Furthermore, the threshold values of SIF range were increased respect to the decrease of *R* and *f* in air and NaCl solution, simultaneously.

4.2. Validation of the newly developed CFCP model

Figure 3a and 3b also show the fitting curves of several models for the three different types of loading condition in air and NaCl solution, respectively. As shown in results, the newly developed model, Eqn. (3) describes the fatigue crack propagation behavior very well at every region both in air and NaCl. NASGRO equation shows a limitation to fit the region I of the experimental data when the slope of region II is very low. Across the region, the curves of Wang's equation relatively do not follow the experimental results except the region I in Figure 3b. As in the case of R=f=0.1, the curves of Wang's model are over estimated the da/dN values than Eqn. (3) and NASGRO.

Figure 4a and 4b show the relationships between loading frequency and material parameters of Eqn. (3), $C(f) = \alpha \exp(\beta f)$ and $m(f) = \gamma \ln f + \delta$, respectively in air and NaCl solution. As shown in the results, the levels of both parameters in NaCl are much more larger than those in air. Also, the parameters decrease respect to increase of loading frequency.

Furthermore, as shown in Figure 5, difference between *C(f)* in air and that in NaCl, *ΔC(f),* decreased according to increase of time period per one cycle, *T=1/f*. On the contrary to this, *Δm(f)* increased according to increase of *T*. Larger *T* means the longer exposure time to corrosive environment per single fatigue load cycle. The longer exposure time can be thought that more

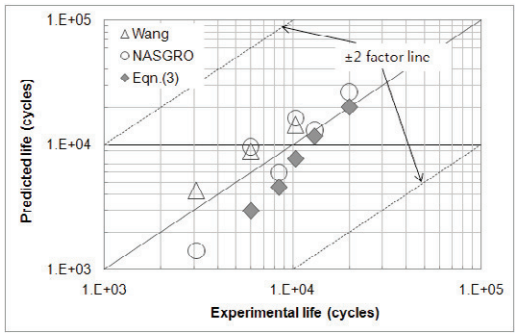

Fig. 6. Experimental and predicted lives of various models.

corrosive effects were applied to the specimen during one load cycle. As in the results, *C(f)* shows increasing corrosion effect respect to increasing exposure time to corrosive environment. However, *m(f)* shows decreasing corrosion effect according to increasing exposure time. As stated previously, it may be possible considered to be the evidences of relating HE mechanism to the parameter *m(f)*, and also relating AD mechanism to *C(f)*.

The life prediction results of each model are shown in Figure 6. As can be seen in the results, the newly developed model, Eqn. (3) shows proper predictions of fatigue lives against experimentally measured data.

5. Conclusions

The FCP and CFCP behaviors of high strength steel, HSB800 were investigated under various loading conditions. Mechanism-based CFCP model for the material was proposed through the modification of Forman equation. The conclusions can be made as follows:

(1) The FCP and CFCP behaviors of HSB800 were experimentally investigated in air and NaCl solution under various loading conditions. The results show that dramatically accelerated CFCP rates appears in NaCl solution comparing with air condition. However, ΔK_{th} and K_{crit} values were not so much changed according to environmental change. Meanwhile, simultaneously increasing R and f leads especially increase of ΔK_{th}.

(2) Newly developed CFCP model additively includes frequency effect and also covers whole range of FCP regions. The model shows a robust effective prediction of FCP and CFCP behaviors by using less number of material parameters than others.

(3) By the evaluation of the parameters used in the model, the effect of corrosion mechanisms was analyzed. Consequently, the parameters *m(f)* and *C(f)* seems to properly represents the corrosion mechanisms HE and AD, respectively.

(4) Predictions of fatigue and corrosion fatigue lives were properly conducted by the comparison with other models. The results show a good agreement to the experimental data.

Acknowledgements

This work was supported by Research Institute of Industrial Science and Technology.

References

[1] KS D 3868:2009. *Rolled steels for bridge structures*. Korean Agency for Technology and Standards 2009.

[2] Gordon DE, Manning SD, Wei RP. *Effects of saltwater environment and loading frequency on crack initiation in 7075-T7651 aluminum alloy and Ti-6Al-4V*. In: Goel VS, editor. Corrosion cracking, Conference proceedings ASM, Salt Lake City: 1985. pp. 157-68.

[3] Hagn L. Life prediction methods for aqueous environments. *Mater Sci Eng A* 1988;**103(1)**:193-205.

[4] Dover WD, Glinka G, Renolds AG, editors. *Fatigue and crack growth in offshore structure*. In: Conf Proc, London, 1986.

[5] Austen IM, Mclntyre P. Corrosion fatigue of high strength steel in low pressure hydrogen gas. *Met Sci* 1979;**13(7)**:420-8.

[6] Zheng XL, Hirt MA. Fatigue crack propagation in steels. *Engng Fract Mech* 1983;**18(5)**:965-73.

[7] NASGRO. *Fracture mechanics and fatigue crack growth analysis software*. NASA Johnson Space Center and Southwest Research Institute.

[8] Wang R. A fracture model of corrosion fatigue crack propagation of aluminum alloys based on the material elements fracture ahead of a crack tip. *Int J Fatigue* 2008;**30**:1376-86.

[9] Forman RG. Study of fatigue crack initiation from flaws using fracture mechanics theory. *Engng Fract Mech* 1972;**4(2)**:333-45.

[10] Hartman A, Schijve J. The effects of environment and load frequency on the crack propagation law for macro fatigue crack growth in aluminum alloys. *Enngg Fract Mech* 1970;**1(4)**:615-31.

[11] Elber W. Fatigue crack closure under cyclic tension. *Engng Fract Mech* 1970;**2**:37-45.

[12] Chen GS, Duquette DJ. Corrosion fatigue of a precipitation-hardened Al-Li-Zr alloy in a 0.5 M sodium chloride solution. *Metall Trans* 1992;**23A(5)**:1563-72.

[13] Ruiz J, Elices M. Environmental fatigue in a 7000 series aluminum alloy. *Corros Sci* 1996;**38(10)**:1815-37.